Tectonophysics 472 (2009) 226–237

Contents lists available at ScienceDirect

Tectonophysics

journal homepage: www.elsevier.com/locate/tecto

2D-3C high-resolution seismic data from the Abitibi Greenstone Belt, Canada

David B. Snyder [a,*], Peter Cary [b], Matt Salisbury [c]

[a] Geological Survey of Canada, 615 Booth Street, Ottawa, ON, Canada K1A 0E9
[b] Sensor Geophysical Ltd., 1300 736 – 6th Avenue SW, Calgary, AB Canada T2P 3T7
[c] Geological Survey of Canada, Bedford Institute of Oceanography, P. O. Box 1006, Dartmouth, NS, Canada B2Y 4A2

ARTICLE INFO

Article history:
Received 21 February 2007
Received in revised form 6 May 2008
Accepted 15 May 2008
Available online 8 June 2008

Keywords:
Three-component seismic reflection data
P–S conversions
Poisson's ratio
Shallow seismic tomography
Abitibi greenstone belt
Mineral exploration

ABSTRACT

One high-resolution seismic profile acquired as part of a 3-component (three orthogonal seismometers) regional seismic reflection survey within the southern Abitibi greenstone belt was investigated in more detail using tomography and by processing all three components. Several high-resolution lines had targeted the Porcupine–Destor deformation zone, a zone proximal to the large gold deposits of the Timmins mining camp, and revealed by the new seismic data to be a composite of early fold structures and late transpressive fault arrays that host quartz-vein gold. Processing of the horizontal-component data assumed that seismic waves were converted from P-waves to S-waves between Vibrator source and receivers; S-wave static corrections proved especially important. Radial-component sections showed most features observed previously on vertical-component sections, but some amplitudes became enhanced, others reduced. The transverse-component stack demonstrated that a few structures are 3-D or contain significant seismic anisotropy. Two dimensional, P- and S-wave travel-time tomography analysis using data from the 10-km-long linear receiver array revealed low-resolution (>200 m) physical property variations, possibly related to mineralization in near-surface structures of the Porcupine–Destor deformation zone; these variations were especially apparent using Poisson's ratio.

1. Introduction

The main purpose of using dual acquisition modes and 3-component seismometers in the "Discover Abitibi" reflection profiling seismic survey was to image regional stratigraphy, major structures, and lithology related to gold and base-metal mineralization in this prolific part of the southern Abitibi greenstone belt (Reed et al., 2005; Snyder et al., 2008). Regional profiles provided guidelines for finding such deposits by better defining the stratigraphic or structural setting; in the high-resolution mode, profiles targeted structures along strike from many of the known ore deposits mined in this area and especially beneath areas of glacial (clay and till) cover. Previous reflection seismic profiles in the region acquired by LITHOPROBE (Green et al., 1990; Jackson et al., 1995; Verpaelst et al., 1995; Perron et al., 1997; Calvert and Ludden, 1999; Adam et al., 2000) used single component seismometers and demonstrated the potential for this type of surveying to help develop an understanding of shallow as well as deep crustal structure in Archean crystalline rocks of the Abitibi province (also see Goleby et al., 2004). The use of relatively high-resolution surveys with three orthogonal components recorded at the surface in crystalline rock environments had not been documented previously, but use of three components had proven advantages for utilizing both P- and S-waves in various combinations in borehole surveys (e.g. Cosma et al., 2003; Bellefleur et al., 2004, and references therein).

Initially only data from the vertical seismometer were processed for all the survey's profiles in order to determine which parts of the survey contained both structures of greater interest and higher quality seismic signal. Here we report further study of one 10-km-long seismic profile near Shillington, Ontario (Fig. 1) as a trial in which the data from the two horizontal components were processed largely independent of the previous processing. The new processing did use the identification of several strong reflectors defining fold and fault structures during processing of the vertical-sensor component data to direct its parameter testing.

The additional processing addressed questions of whether structures of particular interest might reflect S-waves differently than P-waves. Also described for the first time in an analysis of the data set is the use of both P- and S-wave first arrivals in two-dimensional travel-time inversion to: (1) determine structures as defined independently of reflectivity, and (2) estimate bulk physical properties on a broader scale within the uppermost kilometer based on variation of Poisson's ratio. The other seismic profiles in this survey did not display such clearly defined structures at shallow depths and to date their horizontal components have not been deemed worth processing because the main purpose here is to interpret potential mineralized zones that are controlled by such structures.

2. Regional setting

The Abitibi greenstone belt (MERQ-OGS, 1983; Ludden et al., 1986; Jackson and Fyon, 1991; Corfu, 1993) is the largest preserved

* Corresponding author.
E-mail address: dsnyder@NRCan.gc.ca (D.B. Snyder).

0040-1951/$ – see front matter.
doi:10.1016/j.tecto.2008.05.038

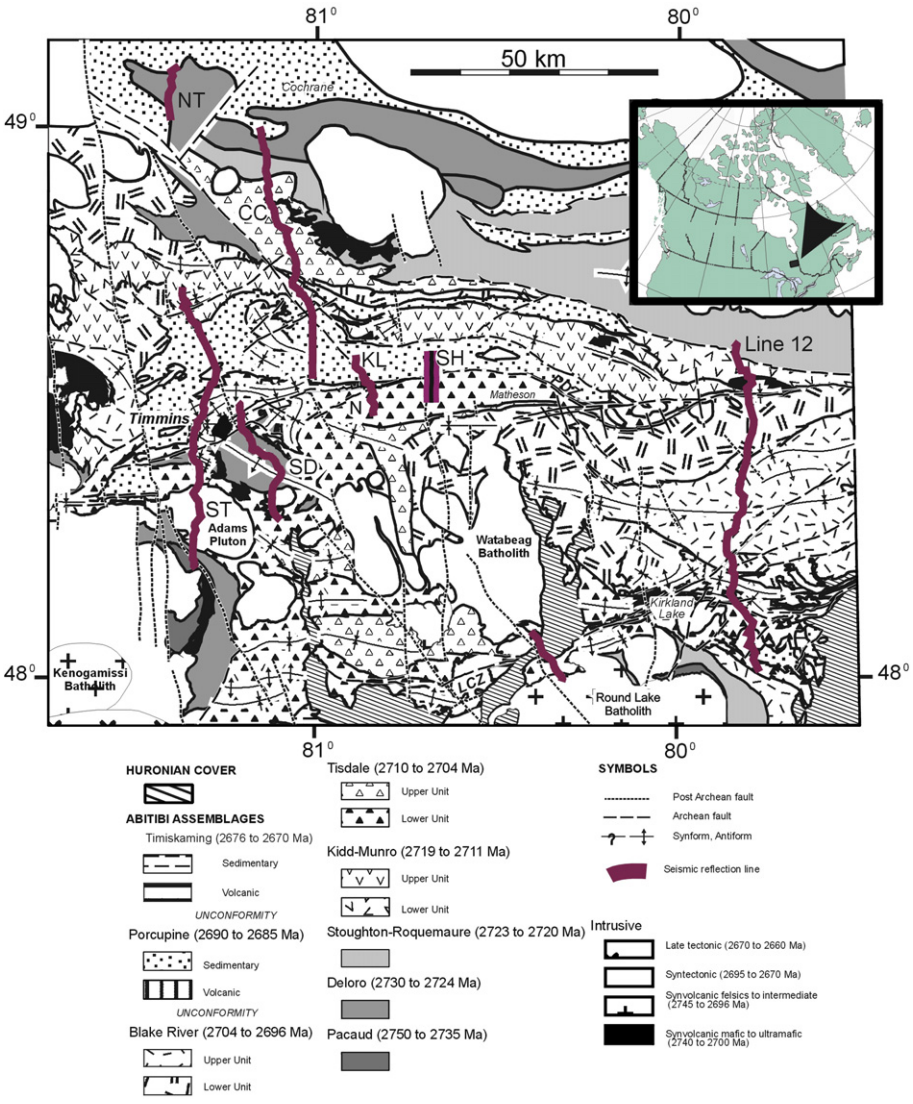

Fig. 1. Location map of the Shillington (SH) and other seismic reflection lines (heavy lines) within the Abitibi greenstone belt of Canada (insert). CC is Crawchest seismic profile, KL is Kettle Lake seismic profile, LCZ is a segment of the Larder Lake–Cadillac deformation zone, N is Nighthawk Lake area, NT is North Timmins seismic profile, PDZ is a segment of the Porcupine–Destor deformation zone, SD is Shaw Dome, ST is South Timmins seismic profile.

greenstone belt in the world, trending generally east–west across the southern Superior craton of North America (Fig. 1). In the east, it is truncated by the ca. 1 Ga Grenville Front tectonic zone. In the west, the Abitibi belt proper is truncated by a major Paleoproterozoic intracratonic thrust, the Kapuskasing Zone, that exposes a gently west-dipping crustal section. Further west within the Kapuskasing Zone, at high structural levels within the dipping crustal section and approximately on strike, the continuation of the Abitibi greenstone belt reappears as the Wawa subprovince. The Abitibi greenstone belt represents a remnant from an originally much larger Neoarchean granite–greenstone terrain that recorded rapid crustal growth in the Neoarchean (e.g., Card, 1990; Percival et al., 2004).

The area is a typical late Archean "granite–greenstone terrain", characterized by polycyclic volcanic stratigraphy overlain by a late-stage sequence of turbiditic sedimentary rocks and finally syn-orogenic clastic rocks (Fig. 1). Numerous granitoid plutons intruded and deformed these rocks in several phases of folding and faulting (Fig. 2). Most volcanic rocks are isotopically juvenile (e.g., Corfu and Noble, 1992; Ayer et al., 2002). Rare and subtle traces of ca. 2.8–2.9 Ga basement involvement occur (e.g., Barrie and Davis, 1990), direct examples of which are exposed in the Kapuskasing Zone (Moser et al., 1996) and to the north of the Abitibi in the Opatica gneiss belt (e.g., Davis et al., 1995).

The regional stratigraphy of the southern Abitibi greenstone belt in this part of Canada is relatively well known and constrained by numerous absolute age dates (Ayer et al., 2002, 2005a,b). Seven of the main assemblages mapped regionally are of relevance to the seismic survey (Fig. 1). The 2750–35 Ma Pacaud, 2730–24 Ma Deloro, 2723–20 Ma Stoughton–Roquemaure, 2718–10 Ma Kidd–Munro, 2710–03 Ma Tisdale, and 2704–2696 Ma Blake River assemblages are predominantly composed of ultramafic to mafic volcanic rocks, commonly pillowed, and pillow lava flows with minor intermediate and felsic volcanic units. These assemblages are unconformably overlain by 2690–85 Ma Porcupine and 2676–70 Ma Timiskaming assemblages which are predominantly sedimentary units representing detritus from the older volcanic units that form turbidites, conglomerates and sandstones generally more felsic in composition than the volcanic substrate.

Plutonic rocks in the region form three groups: synvolcanic, syntectonic, and late-tectonic (Ayer et al., 2005b and references therein). Detailed geochronology demonstrates that some intrusive complexes (e.g. Kenegamissi and Round Lake Batholiths, Fig. 1) formed over 90 Ma by multiple intrusive events. Synvolcanic

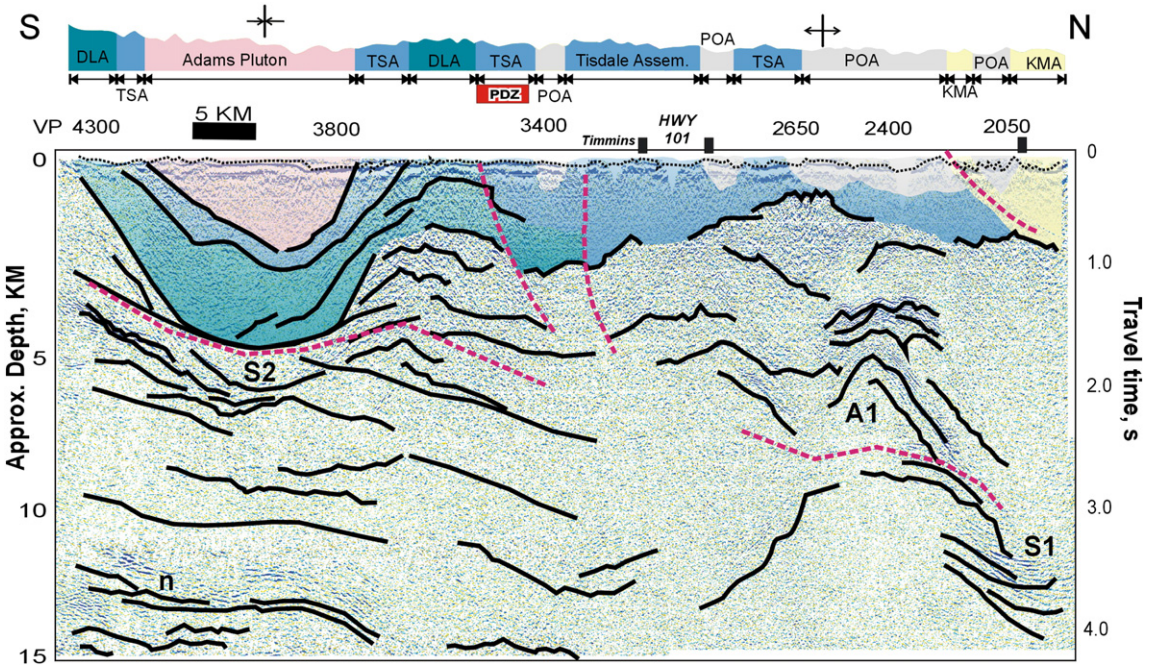

Fig. 2. Reflection profile time section of the South Timmins Line and its interpretation; note depths are approximate. The cross section at the top indicates the rock units and observed strata attitudes as projected onto the seismic line; DLA = Deloro assemblage, TSA = Tisdale assemblage, KMA = Kidd–Munro assemblage, POA = Porcupine assemblage, SRA = Stoughton–Roquemaure assemblage. Solid lines on the interpreted section highlight prominent or laterally continuous reflections; dashed lines are inferred faults. Letters refer to features discussed in the text. Black rectangles represent major gold or base-metal mines located on or near the survey route. PDZ is the Porcupine–Destor deformation zone. Dotted line at top of the seismic section is the base of glacial cover or weathered zone as defined by anomalously low seismic wave speeds.

intrusions range in age from 2745 to 2696 Ma and are coeval with the main volcanic sequences and predate significant horizontal shortening strain. Syntectonic intrusions (e.g. Adams Pluton, Fig. 2) core folds and, as dated between 2695 to 2685 Ma, are coeval with the Porcupine and Timiskaming assemblages and with some of the major deformation episodes in the region. Late tectonic intrusions formed between 2670 and 2660 Ma, typically as batholiths and bysmaliths.

The deformation history is complex and varies within the study area; see Ayer et al. (2005b) and reference therein for a more complete description. The oldest structures recognized regionally are north–south trending folds such as the one cored by the Kenegamissi Batholith (Fig. 1); these folds represent D1 deformation at 2696–2690 Ma that predates deposition of the Porcupine assemblage. East–west trending folds and local south-over-north thrusts represent a D2 phase that forms interference patterns with D1 folds. The prevalence and large amplitudes of these folds and related thrust stacks were clearly defined by the regional seismic reflection profiling (Fig. 2) and analysis of the gravity field (Peschler et al., 2006). This D2 deformation post-dates Porcupine assemblage deposition, but predates Timiskaming assemblage deposition and therefore occurred from 2695 to 2676 Ma. Large-scale D2 folds represent the most readily recognized deformation in the area. Three deformation phases post-date Timiskaming assemblage deposition and are mostly recognized as strains associated with transpression within the Porcupine–Destor Zone (PDZ in Fig. 1). The earliest of these strains, D3, relates to left-lateral displacement on the PDZ and to gold mineralization between 2671–73 Ma (Ayer et al., 2005b).

Table 1
Acquisition parameters.

Parameter	Regional mode	High-resolution mode
Record length	12 s	6 s
Sample interval	2 ms	2 ms
Channels	961 maximum	795 maximum
Geophones	I/O VectorSeis SVSM, a single 3-component phone	
Group interval	25 m	12.5 m
Source	3–4 vibrators over 27 m	2 vibrators over 18 m
	6 sweeps of 28 s	3 sweeps of 28 s
	10–96 Hz linear sweep	10–160 Hz non-linear
Source interval	50 m	25 m
Nominal spread	12,000–0–12,000 m	6000–0–6000 m
Nominal fold	240,000%	24,000%
Filters	1/2 Nyquist, minimum phase with notch out	

Table 2
Processing stream for regional lines.

SEG-Y reformat	
Geometry and crooked line (CDP) binning	
Trace kills	
Spherical divergence amplitude correction	
Spiking deconvolution: 100 ms operator, design window offset dependent	
Refraction statics correction; 300 m datum elevation, 6000 m/s velocity	
Velocity analysis	
Surface-consistent statics	
Shot-domain f–k polygon filter after temporary NMO and AGC	
Receiver-domain f–k polygon filter after temporary NMO and AGC	
Spiking deconvolution: 100 ms operator, design window offset dependent	
Time-variant spectral whitening with bandwidth 4/10–96/120 Hz	
Velocity analysis	
Surface-consistent statics	
Normal moveout correction	
Automatic gain control with 1000 ms window	
CDP stack within common offset bins: 12.5 m spacing	
f–x predictive filter	
Automatic gain control with 1000 ms window	
Dip moveout correction	
Front mutes	
Automatic gain control with 1000 ms window	
CDP stack	
Anisotropic diffusion filter	
Time-variant bandpass filter:	5/10–100/120 Hz @ 0–2 s
	5/10–40/60 Hz @ 3.5–12 s
Trace equalization	
Implicit finite-difference time migration: 0–65°	
Bandpass filter: 10/20–120/140 Hz	

The Porcupine–Destor Zone can be traced over 450 km as characterized by generally steep structures in outcrop. Few systematic differences in metamorphic grade occur across the deformation zone in broadly similar rock assemblages. Synclinally infolded panels of Timiskaming assemblage are truncated by this zone and thus require that some of its deformation postdated deposition of this assemblage. No pluton is known to stitch the fault. Gold mineralization is concentrated along minor faults, especially in S-shaped bends of the main zone (Peschler et al., 2006). Kinematic information is conflicting, but consistent with left-lateral D3 strain followed by right-lateral D4 strain.

3. Acquisition and processing of vertical-component seismic data

Crustal-scale seismic reflection profiles were acquired using Vibroseis sources as part of the multi-disciplinary Discover Abitibi Project (Ayer et al., 2005b; Reed et al., 2005). The survey lines were oriented north–south across major geological trends; from the northern edge of the Abitibi greenstone belt, 82 km north of Timmins, to volcanic rocks and granites located 30 km south of Timmins (Fig. 1). Five parallel transects of variable lengths were located from the city of Timmins in the west to the hamlet of Shillington 48.5 km to the east, and across the major structural zone of the Porcupine–Destor deformation zone at four locations.

The deep seismic reflection profiles were acquired using two modes (Table 1; Fig. 1). Four lines with a total length of 153 line kilometers were surveyed in a regional mode; five lines with a total length of 51 km were surveyed in a high-resolution mode (also see Bergman et al., 2002). The 10-km-long Shillington high-resolution line, shown in Fig. 1, was chosen for converted-wave (P–S) processing because it contained shallow, laterally continuous structures defined by high-amplitude reflections. On this line the vibrator sweep was non-linear, +3 dB/Octave boost, over the frequency band 10–160 Hz. The listen time was 34 s with a 28 s sweep.

Survey lines were located along available roads (mostly gravel) that crossed desired geological targets. The high-resolution lines, such as the Shillington line, employed two vibrators, whereas the regional lines used three vibrators. Single geophones at each station had three sensors: one oriented vertically and two horizontally, as north–south and east–west components. Overburden/bedrock interfaces at a few hundred meters depths are resolved on most sections. Strong crustal reflections appear from 0.5 s (less than 1500 m) to as much as 7 s (about 21 km). Some sections show bedrock responses as shallow as 0.2 s (less than 600 m) or 0.3 s, although these shallower responses are generally weaker. Final stacked sections included processing with several types of static corrections, DMO (Dip Move Out), migration and several stages of bandpass filtering (Table 2). Bandpass filtering tests demonstrated that all source frequencies (10–160 Hz) were recorded as coherent reflections from reflectors as deep as 1.6 s two-way travel time, or about 4.8 km depth.

4. Previous structural interpretation of the vertical-component seismic section

The Shillington high-resolution line (Fig. 3) is the 2004 survey's easternmost crossing of the PDZ, located about 50 km east of Timmins and 80 km west of the 1995 LITHOPROBE (Green et al., 1990) Line 12 (Fig. 1). The mapped trace of the PDZ intersects the profile near VP 500 and separates Tisdale assemblage rocks to the south from Porcupine assemblage rocks to the north (Fig. 3a). The Tisdale assemblage rocks are inferred to host parallel southward dipping reflections everywhere south of the PDZ, and the northernmost reflectors in this set may mark the southern margin of the PDZ (Fig. 3a). At approximately 1.0 s, the

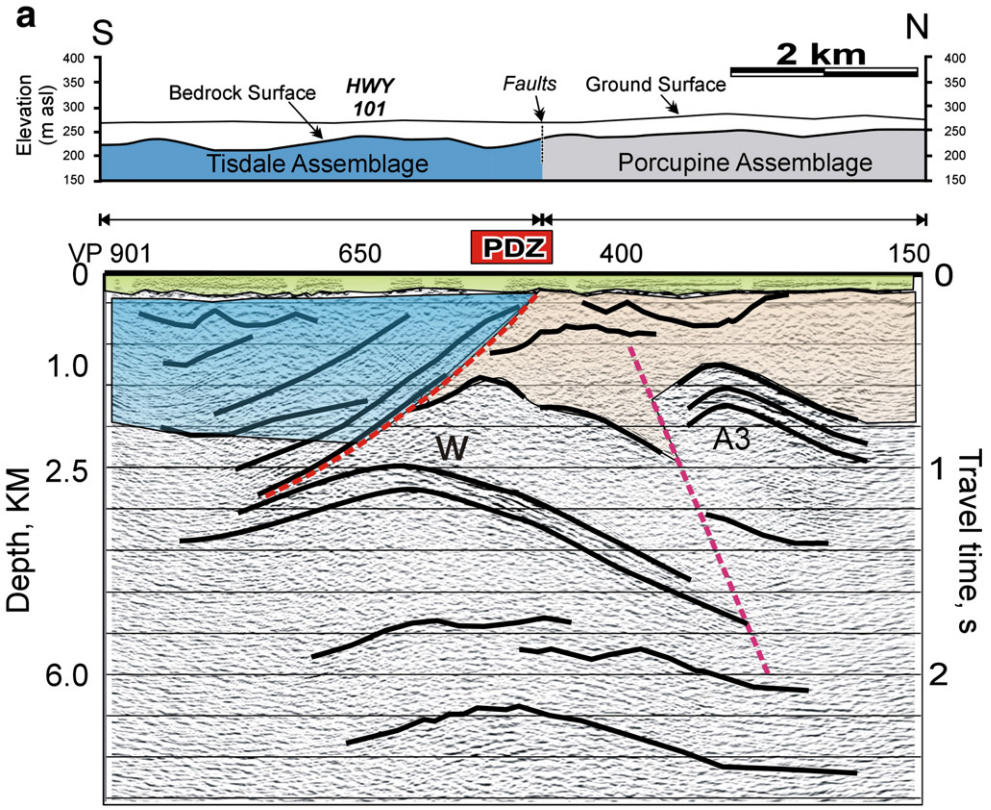

Fig. 3. (a) Interpretation of the Shillington profile. PDZ is the Porcupine–Destor deformation zone. About 150 m of clay or till overburden is defined by the light green–yellow color and closely spaced, near-horizontal reflectors across the entire top of the section. Prominent reflectors define anticlines (A3 and below wedge W) at 1–3 km depths on both sides of the PDZ. (b) Migrated stack of vertical component. (c) Migrated stack of radial component. (d) Unmigrated stack of transverse component. (For interpretation of the references to color in this figure legend, the reader is referred to the web version of this article.)

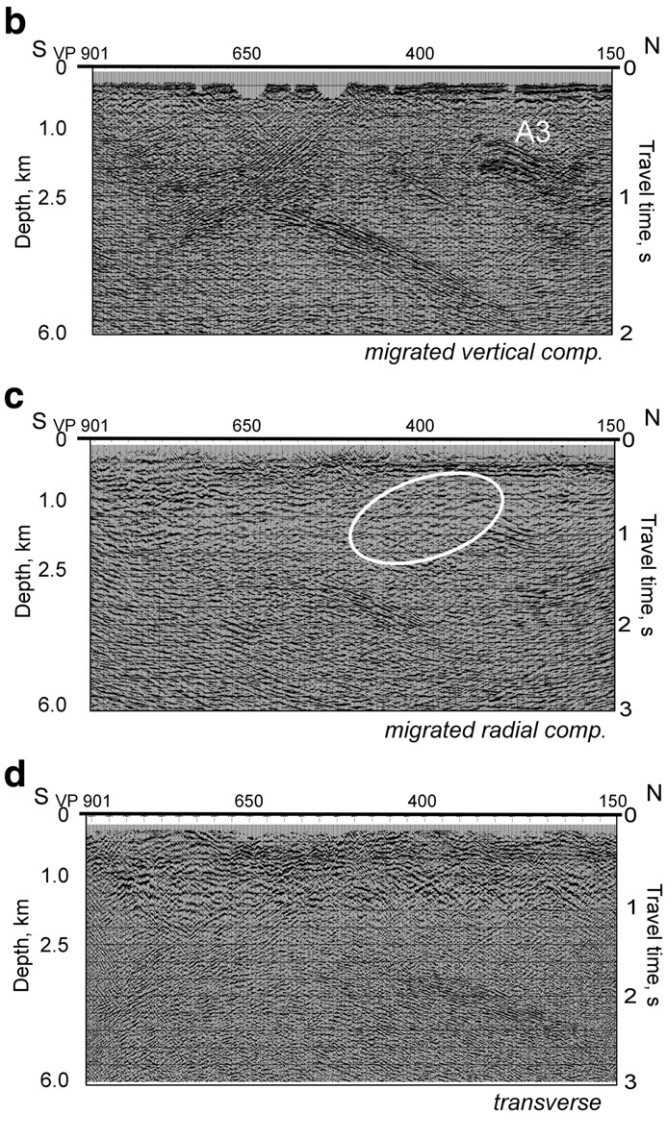

Fig. 3 (*continued*).

deepest of these south-dipping reflections appear deflected into a northward dipping group of reflections (VPs 380, 1.75 s to 640, 1.0 s) to define a wedge-shaped structure (w in Fig. 3a). This and other deflected reflectors suggest that here the shallow PDZ is a thrust dipping moderately to the south.

The most prominent feature occurs at VP 200–300, 0.5–0.7 s as arcs of high-amplitude reflections. Along strike and 30 km to the west, the Tisdale assemblage crops out in the core of an anticline (Fig. 1) and thus is demonstrated to underlie the Porcupine assemblage. An along-strike continuation of this antiform is interpreted as a strongly reflective fold structure on the Shillington seismic section (A3 in Fig. 3a). This feature appears to be offset vertically from the deeper northward dipping reflections described above; this offset implies a reverse fault dipping steeply to the north that projects to the surface north of the PDZ (at VP 420); it may be a subsidiary fault related to later movements on the PDZ (Bleeker, 1995), but with an opposing dip and sense of displacement. Some relatively high-amplitude horizontal reflectors occur in the core of this A3 fold and may represent residual deposits from ca. 2670 Ma metasomatic fluids identified elsewhere in the region and that were trapped locally by this anticline structure.

The north–south Kettle Lakes line (not shown) is also centred on the PDZ and Highway 101 about 30 km east of Timmins (KL in Fig. 1). This area is thought to have 100–200 m of glacial sand cover and >0.2 s of horizontal reflections at the top of the section mark this thicker layer of overburden. Sand is well known to attenuate seismic wave energy and this section looks like a much-subdued version of the Shillington seismic section. This similarity establishes along-strike continuity of structures along this segment of the PDZ as interpreted from reflection geometries; it also confirms fold structures inferred from surface mapping and borehole data.

5. Physical property data base

Laboratory measurements of density and seismic P- and S-wave velocities within representative samples from the Abitibi area indicate a bimodal grouping into volcanic and sedimentary rock types that is useful for seismic interpretations of these rocks (Salisbury et al., 2000, 2003; Reed et al., 2005). In other words, the highest amplitude reflections would be expected where rocks from the first group of largely mafic–ultramafic volcanic Abitibi assemblages are in contact with plutonic or sedimentary rocks from the second group or are intruded into and thus interlayered with felsic-intermediate volcanic rocks.

Measurements of both P- and S-waves allow calculation of bulk Poisson's ratio for these rocks (Fig. 4). Poisson's ratio is generally considered to be most sensitive to quartz (values as low as 0.08) and mafic (high values >0.28) content (Holbrook et al., 1988, 1992; White et al., 1992; Christensen, 1996). In the Abitibi greenstone setting, these two rock types have close association with gold and base-metal mineralization so that Poisson's ratio has good potential as an exploration guide. In studies of specific ores found in this setting (Salisbury et al., 2003), rocks containing more than half iron sulfides, pyrite and pyrrhotite, have Poisson's ratios <0.20, whereas chalcopyrite ($CuFeS_2$) and sphalerite (ZnS) ore has Poisson's ratios >0.30. These values are distinctive from those of all common crustal rocks (Fig. 4).

6. Methodology: horizontal-component processing

The presence of high-amplitude and laterally coherent reflections on the Shillington vertical-sensor seismic section made this line the strongest candidate for processing of data recorded on the two horizontal-sensor components. The final processed seismic image of horizontal-sensor components has good signal-to-noise ratio and displays most of the features observed on the vertical-sensor section (Fig. 3). A novel method of estimating the large shear statics was crucial to the processing, therefore the horizontal-sensor data were processed using a very different processing flow from that of the vertical-sensor data (Tables 2 and 3). Because the Shillington line is oriented north–south, the N-pointing sensor records seismic waves travelling in the plane containing source and receiver points and becomes the radial-sensor component. Similarly, the east-pointing sensor becomes the transverse sensor component of the data. The radial-sensor component was processed first. Processing of the transverse component followed because it used the velocities and statics calculated for the radial-sensor data.

Direct comparison of the vertical-sensor (assumed P-wave) and radial-sensor (assumed S-wave) stacked sections, migrated and displayed in the same way (Fig. 3b and c), reveals selective attenuation of some dips. The radial-component stack has strongly reduced amplitude and coherency of most south-dipping reflections also observed on the vertical stack. The prominent anticline structure at VP 300 and 0.6 s on the vertical-component stack (A3 on Fig. 3) appears as only north-dipping reflectors on the radial component. A prominent sequence of south-dipping reflections south of VP 550 on the vertical-component stack largely disappear on the radial-component stack. The cause of this apparent dip filtering is unknown but may be related to the new effective binning strategy that results from P–S conversion points being slightly displaced from P–P reflections originating at the same source point.

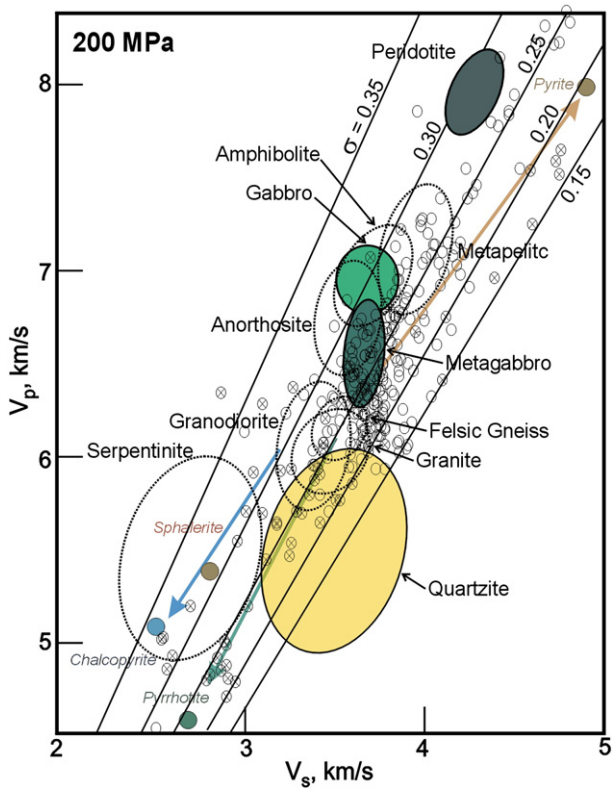

Fig. 4. Summary plot of laboratory measurements of Vp and Vs seismic wave speeds in samples of typical rock types (open circles) (Holbrook et al., 1992; Christensen, 1996) and ore samples (circles with x) (Salisbury et al., 2003; Wang et al., 2005a,b) at 200 MPa pressure. Contours labeled σ are lines of constant Poisson's ratios. Arrows show effect of increasing amounts of sulphide mineralization on seismic wave speeds.

6.1. Shear-wave statics estimation

The crucial step in the processing was estimation of large shear statics that are consistent with each receiver position (Fig. 5). For converted-wave data acquired in a sedimentary basin, these statics are typically on the order of +/−50 to 100 ms. In this dataset acquired within areas with crystalline rock at or near the surface, the shear statics are on the order of +/−70 ms, which is considerably larger than the dominant period of the P–S data. Without a reasonably good estimation of these statics, a coherent stack cannot be obtained.

Most commonly used estimations of shear statics on P–S data rely on the existence of a suite of strong reflectors observed throughout the seismic line, typical in most sedimentary basins (Cary and Eaton, 1993). The Abitibi volcanic rocks do not have enough internal coherent reflectors for the standard method of statics estimation to be of use. Another method depends on the existence of shear-wave refractions that are generated at or near the source (Fig. 5) (Dufour et al., 1996). Although this type of arrival is visible and was used to estimate travel-time of S-waves in tomographic inversions, it is not observed consistently enough near every source point in order to estimate statics. Fortunately another, even more unusual method of statics estimation could be used on these data.

Li (2002) proposed a method of converted-wave statics estimation that uses a strong shear first arrival that is visible shortly after the P-wave first arrival (Figs. 5, 6a). This type of arrival is rare, but in this survey it is presumed to be generated at the large velocity contrast between volcanic rocks and glacial till found in the Shillington area. Fig. 6a, a source record from the radial-component dataset, displays a weak first arrival followed by a much stronger secondary arrival. Fig. 6b shows the corresponding vertical source record and the arrival times of the weak arrival in Fig. 6a clearly corresponds to the P-wave arrival in Fig. 6b. We interpret the strong secondary arrival as a refraction arrival that travels as a P-wave until it encounters the low-velocity, near-surface layer below each receiver, where it converts to a shear wave.

Li (2002) showed how to use the difference in the arrival time between the P-wave on the vertical component and the S-wave on the radial component to estimate the large shear statics. Li's cross-correlation method of picking the time difference between the P and S arrivals was found to not allow decisive results. Instead a linear moveout of 5500 m/s was applied to each receiver record, and first arrivals then were stacked from 0 to 4000 m offset in order to get a strong arrival for each receiver that is easy to pick compared to the neighbouring receivers. Fig. 7 compares the radial-component stack of first arrivals with the vertical-component stack of first arrivals, each with the corresponding P- and S-wave first arrival picks. The receiver-consistent shear statics were computed from the difference between the two.

6.2. P–S DMO

Another important step in the processing of the P–S data was the application of P–S dip moveout (DMO). Dip moveout compensates for reflection point dispersal due to dipping reflectors and removes the dip-dependence of stacking velocities. It also can act as an effective noise attenuator, especially if the data are very noisy. Fig. 8 shows the asymptotic common-conversion-point (CCP) stack of the radial component with f–x noise attenuation applied. Fig. 9 shows the P–S DMO stack of the radial component. Comparison of Figs. 8 and 9 reveals a change in the position and coherence of a few dipping events (see white arrow at about 2 s between VPs 400–600) after DMO was applied, also improved coherency of flat events near the surface, as well as a general improvement in the signal-to-noise ratio of the image. The radial-component stack does appear to define reflectors with greater resolution.

Table 3
Radial and transverse-component processing summary.

Assign geometry to inline and crossline components in exactly the same way as for the vertical component
Rotation from inline/crossline components to radial/transverse components
Selection of a radial component for further processing
Asymptotic CCP binning
Inspection of data for exclusion of noisy traces and noisy receivers
Amplitude recovery, spherical divergence correction $1/tv^2$
Surface-consistent deconvolution
Vibroseis deconvolution compensation
Trace-by-trace time-variant spectral whitening
Application of refraction statics as determined from vertical component
Application of receiver-consistent statics calculated from secondary shear arrival after P-wave first break
Calculation and application of surface-consistent residual statics (stack-power maximization method)
Normal moveout correct
Trace muting
Automatic gain control (AGC)
Apply static to move to final datum
Gather and partially stack data into constant-offset sections
f–x deconvolution noise attenuation of constant-offset sections
AGC
Apply static to move to floating datum
Apply converted-wave dip moveout (P–S dmo with Vp/Vs = 1.9)
Post-dmo trace kills at ends of constant-offset sections
Stack constant-offset sections
Time-variant spectral whitening
Trace equalization
f–x deconvolution noise attenuation
Implicit finite-difference time migration
Bandpass frequency filtering
Time-variant scaling

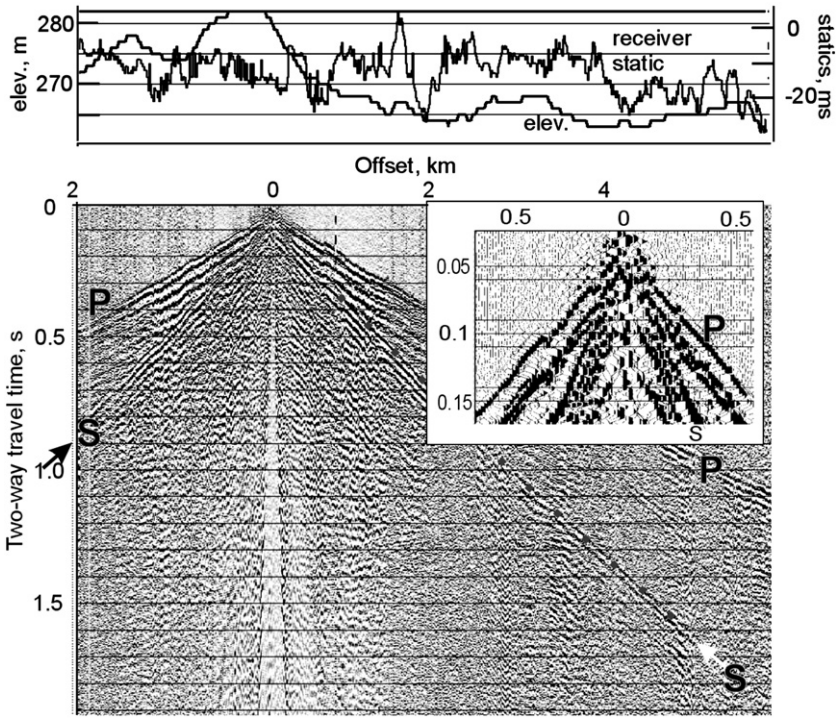

Fig. 5. Vibrator point gather for VP 295, located above anticline structure, that illustrates quality of S-wave arrivals used in tomography analysis. White arrow indicates S-waves with 3400 m/s velocity; black arrow shows S-waves with 3100 m/s velocity. P-wave first breaks have associated velocities of 6100–6600 m/s. Inset shows near-source records and indicates that S-waves originated <52 ms after P-waves and thus P–S conversions occurred at very shallow depth beneath the vibrators. Surface elevation and P-wave receiver statics are shown at top.

6.3. Transverse component

The transverse component is perpendicular to the radial component. In a two-dimensional isotropic earth, there would be no signal on the transverse component. In practice there is always some coherent energy recorded on the transverse component due to shear-wave splitting from anisotropy and three-dimensional structures that cause off-line scattering and out-of-plane reflections or both. Transverse-component source gathers showed few coherent reflections and are therefore not illustrated. The transverse component, processed to structure stack using the velocities and statics from the radial component displays some coherent reflections as expected (Fig. 3d).

7. Methodology: 2-D tomography

7.1. 2-D tomographic inversion methods

First arrival times of direct P-wave energy at each recording position (so-called first breaks) were picked to ±6 ms and recorded in the SEG-Y trace headers as part of the main processing sequence (Figs. 5, 7b). S-wave first arrivals were picked specifically for tomographic inversions (Fig. 5).Variations among these arrival times can be used in the 2-D, turning-ray tomographic inversion method to produce a velocity or wave-speed model within the uppermost 1–1.5 km at resolutions approaching the source and receiver spacings (e.g. Zelt et al., 2001; Hole et al., 2006). Theoretical considerations suggest that the smallest feature reconstructed using ray travel-time tomography is approximated by the first Fresnel zone radius for a given wavelength and distance of propagation (Williamson, 1991); here S-waves travelling 400 m at 2500 m/s would have a minimum radius of 200 m. Source spacings used in the analysis are 125–250 m and the final smoothing used is 100 m vertically and 200 m horizontally. In the tomographic models presented here a smoothed starting model was based on one-dimensional velocity functions every 20 CDPs or 125 m. Thus the resolution imposed here by smoothing over 100–200 m is considered consistent with theoretical estimates.

Ray tracing through this starting model was then performed using arrivals from every tenth vibrator point (250 m spacing). Potential

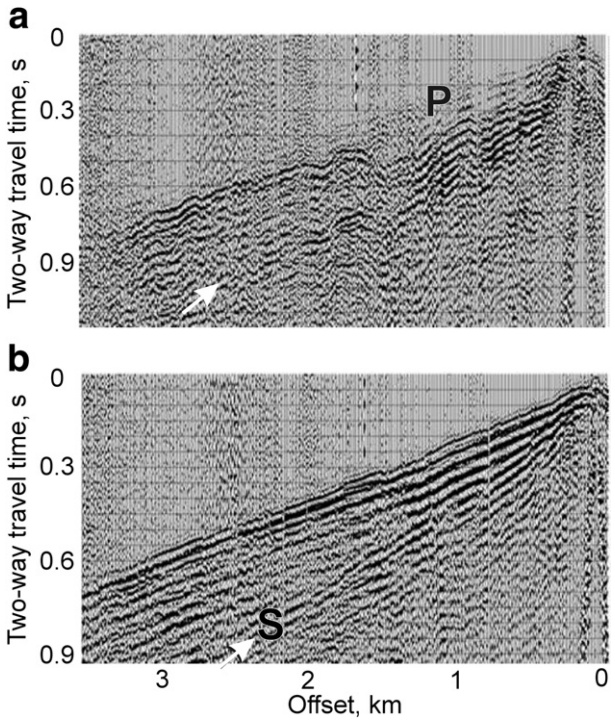

Fig. 6. Representative vibrator point (VP 201) gathers. (a) radial component; (b) vertical component. Offsets range from 0 to 3535 m. White arrows indicate S-wave first arrivals (S); P indicates P-wave first arrivals.

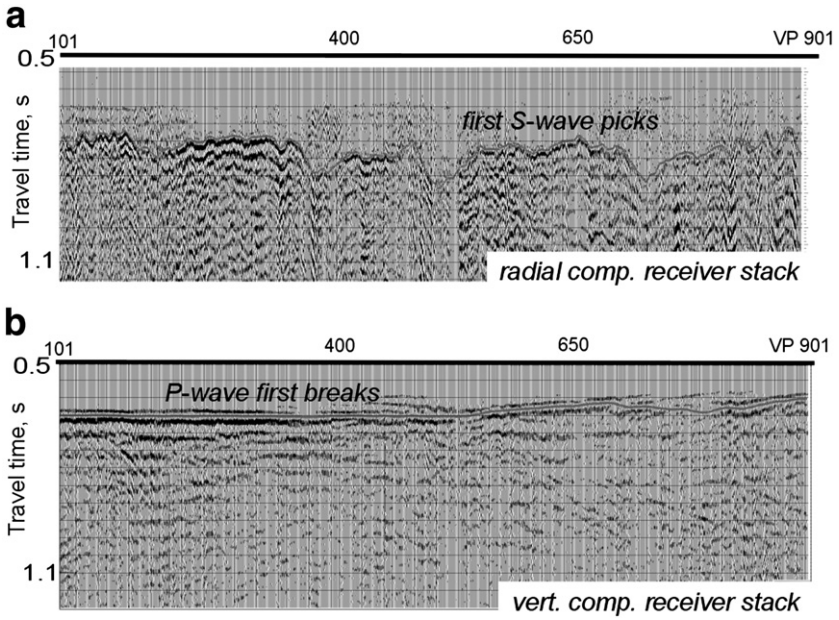

Fig. 7. (a) Asymptotic structure stack of radial component showing S-wave first arrival picks; (b) Vertical-component receiver stack showing P-wave first arrival picks.

model resolution is governed by cell size, here cells were 100 m horizontally by 100 m vertically. Using this set of rays (seismic wavepaths), four to five tomographic iterations had decreasing maximum allowed residuals between observed and calculated travel times, typically decreasing from 300 ms to 50 ms, until models had RMS residuals <3 and cell values changed on average less than 100 m/s. Final horizontal and vertical smoothing were typically 200 m and 100 m, respectively. Final ray density within modelling cells ranged from preset minimums of 5–50 to greater than 500.

In surveys with either sparse receivers or sources, uncertainties are often assessed quantitatively either by checkerboard or jackknife tests (White et al., 1992; Hole et al., 2006). Because large numbers of both sources and receivers were available as uniform arrays in this survey, these tests were not performed. Checkerboard tests are more instructive when asymmetrical or variable density source-receiver arrays are used; here both arrays are uniform along the profile. Ray density patterns indicate robust inversions to 500 m depths because turning rays crossed cells at a wide distribution of angles, from near-horizontal to near-vertical (Fig. 10). Deeper parts of the models have lesser ray density and thus are considered less reliable. Maximum resolution is estimated here based on smoothing and cell size, at 200 m horizontal and 100 m vertical, comparable to theoretical

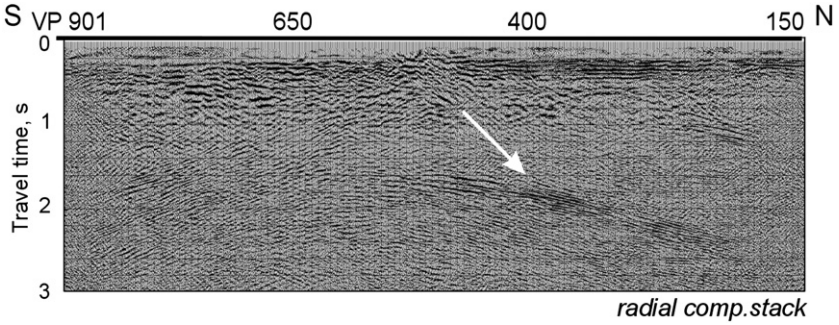

Fig. 8. Radial-component receiver stack showing strong shear first arrival after weak P-wave first arrival. White arrow highlights clearly resolved reflections defining the north limb of the anticline structure.

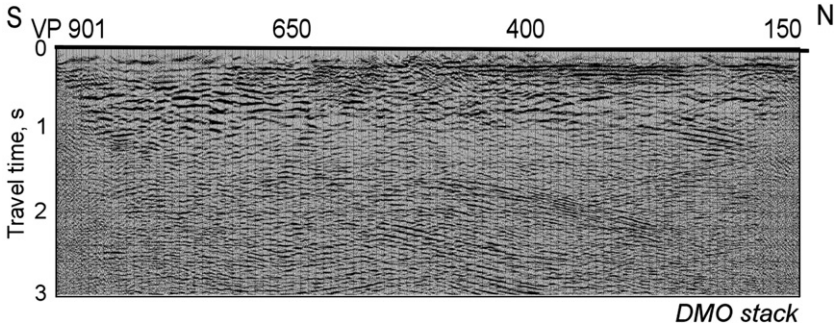

Fig. 9. P–S DMO stack of radial component.

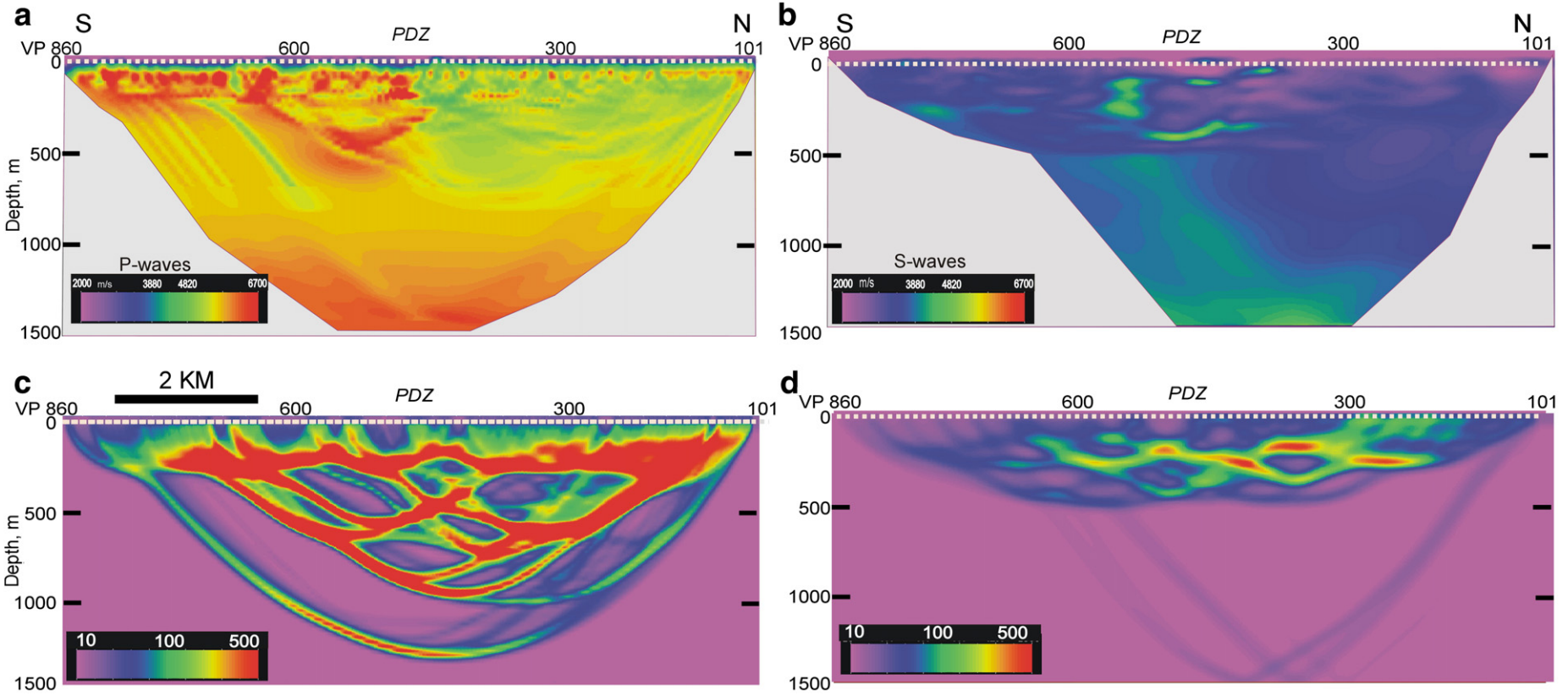

Fig. 10. Results of 2-D travel-time tomography. (a) P-wave velocity model. (b) S-wave velocity model. (c) ray-trace diagram for assumed P-waves first arrivals. (d) Ray-trace diagram for assumed S-wave first arrivals. Uneven ray coverage probably occurs due to channeling of rays by strong near-surface velocity gradients.

considerations (Williamson, 1991). Repeatability of residuals <50 ms and RMS fits <3.0 during the final iterations of tomographic inversion suggests that uncertainties of P- and S-wavespeeds are 1–3%, consistent with previous studies in similar settings (White et al., 1992).

7.2. 2-D tomographic inversion results

Tomographic inversions were performed using both P-wave first arrivals, as represented by the first break picks, and on strong S-wave arrivals (Fig. 5). Ray diagrams of wavepaths through the two starting models demonstrate a greater depth of penetration possible with P-waves using the same source-receiver offsets (Fig. 10). P-wave raypaths show evidence of channeling of rays by near-surface velocity distributions (Bergman et al., 2004), but penetrate to depths of up to 1000 m. S-waves show similar channeling and penetrate to depths of only about 400 m. In both models the smoothing of velocity fields between each iteration reduced the undesirable effects of the ray channeling on the final velocity models. Where constrained by adequate ray densities (>50), both velocity models reveal consistent lateral gradients (velocities decreasing south to north) near the center of the line (VP 550 in Fig. 10) where the Porcupine–Destor Zone is interpreted to cross the profile (Fig. 3). To the north, near-surface sedimentary rocks of the Porcupine assemblage are inferred by these models to have slower P- and S-wave speeds than near-surface mafic volcanic rocks of the Tisdale assemblage to the south (Snyder et al., 2008).

The models of P- and S-wave speed can be combined to produce a model of Poisson's ratio, which is interpreted as sensitive to certain rock types and their key constitutive minerals in low porosity rocks (Fig. 11). The present discussion of Poisson's ratio applies only to model depths less than 400 m where both P- and S- wave models have adequate ray coverage. Low ratios typically indicate high quartz content and high ratios indicate many mafic minerals are present (Fig. 4) (White et al., 1992; Christensen, 1996). Estimated uncertainty in the smoothed values of Poisson's ratio discussed here is high, about 2–4% or ±0.01, based on the uncertainty estimates for P- and S-wave speeds. Relative uncertainties are much less, so that lateral and vertical variations in the Poisson's ratio model for shallow parts of the Shillington line appear to be statistically significant and in places related to rock types inferred to be present (compare Figs. 3 and 11). High ratios may mark mafic and ultramafic (komatiitie) rocks known to occur regionally within the Tisdale assemblage. In other places, unusual Poisson's ratios may be either spurious and due to greater uncertainties related to local poor ray coverage or reliable and indicate that secondary minerals are present, minerals that formed during later metasomatism or by the influx of mineralizing fluids.

8. Additional interpretations from the new processing

Processing horizontal components and use of P- and S-wave direct arrivals to model velocities in the near-surface enables further interpretations of structures and rock distribution beneath the Shillington profile, beyond those possible using only the vertical-component reflection profiles. Much stronger evidence now exists of mafic Tisdale assemblage rocks at shallow depth north of the Porcupine–Destor Zone. S-wave conversions and tomographic models provide good estimates of clay and glacial till cover thicknesses along the profile. A combination of the P- and S-wave velocity models reveals possible distributions of sulphide deposits and some of their typical host rocks.

The new P-wave tomographic model most clearly indicates a change in rock types across the Porcupine–Destor Zone (Fig. 10a); P-wave speeds decrease from >6 km/s to <4 km/s in the uppermost 500 m over a horizontal distance of <500 m. This sharp gradient appears to move slowly northward with depth, counter to the boundary between Tisdale assemblage volcanic rocks interpreted from the vertical-component reflection section (Fig. 3a). The trend of the gradient is consistent with the inferred rock types (Fig. 4), but its location at depth is not. Tisdale assemblage rocks may therefore occur at a shallow depth across the entire profile and internal variation in rock types among felsic, intermediate and komatiitic rocks within the Tisdale assemblage may better explain the observed P-wave velocity trends. The original interpretation based on only the vertical components was thus overly simple.

The strong reflectors that define the anticline structure (A3 on Fig. 3) most probably represent a series of komatiite flows that were mapped regionally within the Tisdale assemblage. These flows are typically several meters thick individually and tens of meters thick as a composite unit. The composite unit thus lies at the threshold of resolution for the P- and S-waves used in this survey. The flows would appear as strong reflectors to the P-waves, but less strongly as P to S converters–reflectors, especially since the fold wavelengths are similar to the relevant seismic wave Fresnel zones of about 200 m. This could explain the observed differences in reflectivity between vertical and radial components (Fig. 3).

The radial-component static correction estimation and the P-wave tomographic model both provide strong, new constraints on the thickness of the low-velocity clay and glacial till cover thickness along the profile. The P-wave velocities display a consistent thinning of this cover from about 65 m in the south to 30 m in the north. The static corrections (50–100 ms) suggest similar thicknesses of 50–100 m. Local topography observed on this subcrop surface should channel some of the rays used in the tomography study (Bergman et al., 2004). One such feature occurs at VP 640 (Fig. 10a).

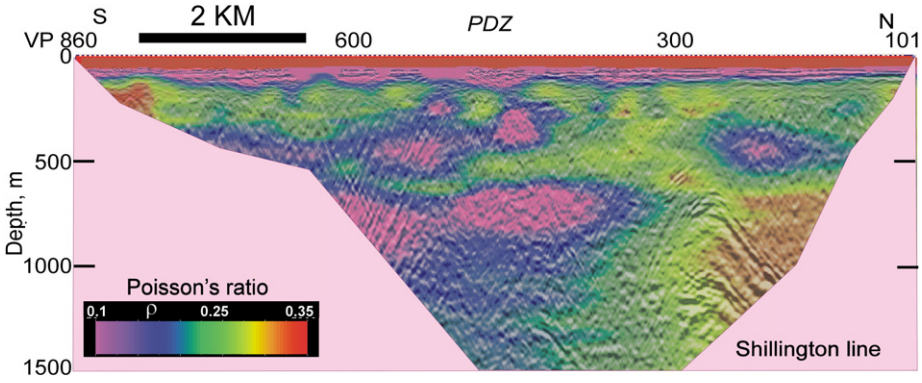

Fig. 11. Poisson's ratio model for the Shillington line. Red colors are relatively high ratios, typical of mafic rocks and some sulfides such as pyrite; purple and blue colors are low ratios typical of relatively silica-rich rocks such as quartz and many sulphide mineralizations. Background seismic reflection section is that of Fig. 3b.

Quartz and quartz-rich rocks have Poisson's ratios <0.25 (Fig. 4) and values <0.20 appear near the Porcupine–Destor Zone (PDZ) at several depths (Fig. 11), suggesting the presence of felsic rocks if these values are taken as representative values. Poisson's ratios greater than 0.28 suggest that gabbro, ultramafic rocks, serpentinites, or perhaps massive sulphides such as chalcopyrite or sphalerite are present near or above the anticline structure beneath VP 300 and to the north. If Tisdale or Kidd–Munro assemblage rocks underlie the Porcupine assemblage (Figs. 1 and 3), basalt (gabbro field in Fig. 4) and komatiite (peridotite field in Fig. 4) lava flows common in these units provide probable sources of the high Poisson's ratios. Silicification, carbonization and introduction of sulphide minerals typically do not cause strong gradients in physical properties and thus would be largely invisible to the seismic methods initially used to interpret this profile.

9. Discussion and summary

Resolving structures defined by seismic waves traveling within crystalline rocks is widely acknowledged as challenging. Here, key structures within the Abitibi greenstone belt were first identified and located using both regional and high-resolution seismic reflection profiling data from vertical-component geophones only. Subsequent additional processing of selective features using the horizontal components required the use of seldom observed seismic phases to do the necessary static corrections. Although we interpret these new converted-wave sections to represent seismic phases largely distinct from the original vertical-component stacked sections, those structures interpreted from these equivalent sections are nearly identical, albeit much fewer in number. The vertical-component sections contain regional-scale structures that have clarified thinking about the tectonic history of a major tectonic feature, the Porcupine–Destor Zone (PDZ), by showing south-dipping reflectors related to early thrusting and wedging, late north-dipping reverse faulting due to transpressional strain, and locally horizontal reflectors that might represent very late-stage silicification, carbonization or mineralization within structural fluid traps such as anticlines. Radial-component sections show only a few, minor parts of these structures but reveal some weak, south-dipping reflectors north of the PDZ (Fig. 3c) that might indicate older fold structures in an important location because these early deformation structures were subsequently deformed by strike-slip faulting within the PDZ. The radial-component section also reveals more detail of the basement-cover contact and shows angular unconformity relationships in a few locations. Thickness estimates of the cover sequence are important to mineral exploration in this region.

Both P- and S-wave velocity models derived from diving-ray tomography inversion of the relevant first arrivals displayed apparent anomalies that varied spatially but independent of the reflector structures defined previously. Many anomalies do coincide with or adjoin fault or depositional contacts inferred from interpretation of the vertical- and horizontal-component reflection profile sections; strong velocity and Poisson's ratio variation across the inferred cover-basement unconformity is the clearest example and provides confidence in the overall results and interpretations. The highest values of Poisson's ratio occur above and north of the anticline defined by reflectors and where mafic and ultramafic lava flows of the Tisdale or Kidd–Munro assemblages are expected in the subsurface based on surface mapping. These rock types are consistent with the observed ratios. Along its strike, the Kidd–Munro assemblage also hosts numerous sulfide ore deposits that are also characterized by high Poisson's ratio such as are estimated here.

Other Poisson's ratio anomalies appear less directly related to structures, but are generally located within the PDZ. The anomalies generally have values less than 0.20 and are thus typical of quartz-rich rocks or some sulfide ores. It should be noted that in shallow crust, cracks can also raise or lower the Poisson's ratio, depending on their aspect ratios (Shearer, 1988). These anomalies may therefore point to zones of fault cataclasites, fracture-filling veins or alteration halos traditionally associated with mineralization targets within the Abitibi and that were a primary goal of these recent seismic surveys in a mature mining camp.

Original processing and interpretation of these seismic surveys provided key insights into regional-scale, upper crustal folds and thrust stacks within the Abitibi greenstone belt rocks. Processing of the horizontal components revealed no new structures, but did add new details and clarified interpretations made previously using the vertical components. The differences between the sections inferred to represent P–P reflections versus P–S reflections indicate that subtle differences in reflection location and angle due to P–S conversion may be resolvable and capable of being mapped in a consistent manner. Combined P- and S-wave tomography revealed broader-scale variations of physical properties that appear largely independent of the reflection geometries, but whose interpretation is indicative of prospective rock types and perhaps alteration associated with mineralization in a known, prospective ore setting.

Acknowledgments

The deep seismic reflection profiles were acquired in June and July 2004 by Kinetex, Inc. of Calgary. Sensor Geophysical Ltd. processed these vertical and horizontal data under contract to the Timmins Economical Development Corporation and Natural Resources Canada, respectively. Tomographic inversions were performed using the turning-ray tomography analysis package in Landmark Systems Promax 7.0 seismic processing software (Zhu et al., 1992). D. Brown and B. Goleby gave permission to show physical properties of unpublished sample data. B. Roberts, J. Ayer, G. Bellefleur, and D. White provided useful suggestions to early versions of the manuscript. This paper represents ESS, Geological Survey of Canada Contribution number 20060647 to the Abitibi project of its Targeted Geoscience Initiative III program.

References

Adam, E., Perron, G., Milkereit, B., Wu, J., Calvert, A.J., Salisbury, M., Verpaelst, P., Dion, D.-J., 2000. A review of high-resolution seismic profiling across the Sudbury, Selbaie, Noranda, and Matagami mining camps. Canadian Journal of Earth Science 37, 503–516.

Ayer, J., Amelin, Y., Corfu, F., Kamo, S., Ketchum, J., Kwok, K., Trowell, N., 2002. Evolution of the southern Abitibi greenstone belt based on U-Pb geochronology: autochthonous volcanic construction followed by plutonism, regional deformation and sedimentation. Precambrian Research 115, 63–95.

Ayer, J.A., Berger, B.R., Hall, L.A.F., Houle, M.G., Johns, G.W., Josey, S., Madon, Z., Rainsford, D., Trowell, N.F., Vaillancourt, C., 2005a. Geological compilation of the central Abitibi greenstone belt: Kapuskasing Structural Zone to the Quebec border. Ontario Geological Survey. Preliminary Map P.3565, scale 1:250 000.

Ayer, J.A., Thurston, P.C., Bateman, R., Dubé, B., Gibson, H.L., Hamilton, M.A., Hathaway, B., Hocker, S., Houlé, M., Hudak, G., Lafrance, B., Lesher, C.M., Ispolatov, V., MacDonald, P.J., Péloquin, A.S., Piercey, S.J., Reed, L.E., Thompson, P.H., 2005b. Overview of results from the Greenstone Architecture Project: Discover Abitibi Initiative. OFR 6154.

Barrie, C.T., Davis, D.W., 1990. Timing of magmatism and deformation in the Kamiskotia–Kidd Creek area, Western Abitibi subprovince, Canada. Precambrian Research 46, 217–240.

Bellefleur, G., Müller, C., Snyder, D., Matthews, L., 2004. Downhole seismic imaging of a massive sulfide ore body with mode-converted waves, Halfmile Lake, New Brunswick. Geophysics 69, 318–329.

Bergman, B., Juhlin, C., Palm, H., 2002. High-resolution reflection seismic imaging of the upper crust at Laxemar, southeastern Sweden. Tectonophysics 355, 201–213.

Bergman, B., Tryggvason, A., Juhlin, C., 2004. High-resolution seismic traveltime tomography incorporating static corrections applied to a till-covered bedrock environment. Geophysics 69, 1082–1090. doi:10.1190/1.1778250.

Bleeker, W., 1995. Surface geology of the Porcupine camp. In: Heather, K.B., Percival, J.A., Moser, D., Bleeker, W. (Eds.), Tectonics and metallogeny of Archean crust in the Abitibi–Kapuskasing–Wawa region. Geological Survey of Canada Open File 3141, pp. 13–37.

Calvert, A.J., Ludden, J.N., 1999. Archean continental assembly in the southeastern Superior Province of Canada. Tectonics 18, 412–429.

Card, K.D., 1990. A review of the Superior Province of the Canadian Shield, a product of Archean accretion. Precambrian Research vol. 48, 99–156.

Cary, P.W., Eaton, D.W.S., 1993. A simple method for resolving large converted-wave (P-SV) statics (short note): Geophysics. Society of Exploration Geophysics 58, 429–433.

Christensen, N.I., 1996. Poisson's ratio and crustal seismology. Journal of Geophysical Research 101 (2), 3139–3156.
Corfu, F., 1993. The evolution of the southern Abitibi greenstone belt in light of precise U-Pb geochronology. Economic Geology 88, 1323–1341.
Corfu, F., Noble, S.R., 1992. Genesis of the southern Abitibi greenstone belt, Superior Province, Canada: evidence from zircon Hf isotopic analyses using a single filament technique. Geochimica et Cosmochimica Acta 56, 2081–2097.
Cosma, C., Heikkinen, P., Keskinen, J., 2003. Multiazimuth VSP for rock characterization of deep nuclear waste disposal sites in Finland. In: Eaton, D.W., Milkereit, B., Salisbury, M.H. (Eds.), Hardrock seismic exploration, Society of Exploration Geophysics. Geophysical Developments, vol. 10, pp. 207–226.
Davis, W.J., Machado, N., Gariepy, C., Sawyer, E.W., Benn, K., 1995. U-Pb geochronology of the Opatica tonalite–gneiss belt and its relationship to the Abitibi greenstone belt, Superior Province, Quebec. Canadian Journal of Earth Sciences 32, 113–127.
Dufour, J., Lawton, D.C., Gorek, S., 1996. Determination of S-wave static corrections from S-wave refractions on P–S data. 66th Ann. Internat. Mtg: Society of Exploration Geophysics, pp. 1551–1554.
Goleby, B.R., Blewett, R.S., Korsch, R.J., Champion, D.C., Cassidy, K.F., Jones, L., Groenewald, P.B., Henson, P.A., 2004. Deep seismic reflection profiling in the Archaean northeastern Yilgarn Craton, Western Australia: implications for crustal architecture and mineral potential. Tectonophysics 388, 119–133.
Green, A.G., Milkereit, B., Mayrand, L., Ludden, J.N., Hubert, C., Jackson, S.L., Sutcliffe, R.H., West, G.F., Verpaelst, P., Simard, A., 1990. Deep structure of an Archean greenstone terrane. Nature 344, 327–330.
Holbrook, W.S., Gajewski, D., Krammer, A., Prodehl, C., 1988. An interpretation of wide-angle compressional and shear wave data in southwest Germany">: Poisson's ratio and petrological implications. Journal of Geophysical Research 93 (B10) 12,081–12,106.
Holbrook, W.S., Mooney, W.D., Christensen, N.I., 1992. The seismic velocity structure of the deep continental crust. In: Fountain, D.M., Arculus, R., Kay, R. (Eds.), Continental Lower Crust. Elsevier, New York, pp. 21–43.
Hole, J.A., Ryberg, T., Fuis, G.S., Bleibinhaus, F., Sharma, A.K., 2006. Structure of the San Andreas fault zone at SAFOD from a seismic refraction survey. Geophysical Research Letters 33 (7), L07312. doi:10.1029/2005GL025194.
Jackson, S.L., Fyon, J.A., 1991. The Western Abitibi subprovince in Ontario. In: Thurston, P.C., Williams, H.R., Sutcliffe, R.H., Stott, G.M. (Eds.), Geology of Ontario. Ontario Geological Survey Special, vol. 4, pp. 405–482. Part 1.
Jackson, S.L., Cruden, A.R., White, D., Milkereit, B., 1995. A seismic-reflection-based regional cross section of the southern Abitibi greenstone belt. Canadian Journal of Earth Science 32, 135–148.
Li, Y., 2002. A new method for converted wave statics correction. 72nd Ann. Internat. Mtg: Society of Exploration Geophysics, pp. 979–981.
Ludden, J., Hubert, C., Gariépy, C., 1986. The tectonic evolution of the Abitibi greenstone belt of Canada. Geological Magazine 123, 153–166.
MERQ-OGS, 1983. Lithostratigraphic map of the Abitibi Subprovince. Ontario Geological Survey/Ministere de l'Energie et des Ressources, Quebec, 1:500,000 map, catalogued as Map 2484 in Ontario and DV 83-16 in Quebec.
Moser, D.E., Heaman, L.M., Krogh, T.E., Hanes, J.A., 1996. Intracrustal extension of an Archean orogen revealed using single-grain U-Pb zircon geochronology. Tectonics 15, 1093–1109.
Percival, J.A., Bleeker, W., Cook, F.A., Rivers, T., Ross, G., van Staal, C., 2004. PanLITHOP-ROBE Workshop IV: intra-orogen correlations and comparative orogenic anatomy. Geoscience Canada 31, 23–39.
Perron, G., Milkereit, B., Reed, L.E., Salisbury, M., Adam, E., Wu, J., 1997. Integrated seismic reflection and borehole geophysical studies at Les Mines Selbaie, Quebec. The Canadian Institute of Mining and Metallurgy Bulletin 90, 75–82.
Peschler, A.P., Benn, K., Roest, W.R., 2006. Gold-bearing fault zones related to Late Archean orogenic folding of upper and middle crust in the Abitibi granite–greenstone belt. Ontario. Precambrian Research 151, 143–159.
Reed, L.E., Snyder, D.B., Salisbury, M., 2005. 2D reflection seismic surveying in the Timmins /Kirkland lake area, Northern Ontario, Canada; acquisition, processing, interpretation: Discover Abitibi Initiative. Ontario Geological Survey Open File Report 6169.
Salisbury, M.H., Milkereit, B., Ascough, G., Adair, R., Matthews, L., Schmitt, D.R., Mwenifumbo, J., Eaton, D.W., Wu, J., 2000. Physical properties and seismic imaging of massive sulfides. Geophysics 65, 1882–1889.
Salisbury, M.H., Harvey, C.W., Matthews, L., 2003. The acoustic properties of ores and host rocks in hardrock terranes. In: Eaton, D.W., Milkereit, B., Salisbury, M.H. (Eds.), Hardrock Seismic Exploration. Society of Exploration Geophysicists. Geophysical Developments Series, pp. 9–19. No. 10.
Shearer, P.M., 1988. Cracked media, Poisson's ratio and the structure of the upper oceanic crust. Geophysical Journal Royal Astronomical Society 92, 357–362.
Snyder, D.B., Bleeker, W., Reed, L.E., Ayer, J.A., Houle, M.G., Bateman, R., 2008. Tectonic and metallogenic implications of the Discover Abitibi Regional Seismic Profiles in the Timmins Mining Camp. Economic Geology 103, 1135–1150.
Verpaelst, P., Peloquin, A.S., Adam, E., Barnes, A.E., Ludden, J.N., Dion, D.J., Hubert, C., Milkereit, B., Labrie, M., 1995. Seismic reflection profiles across the mine series in the Noranda camp of the Abitibi belt, Eastern Canada. Canadian Journal of Earth Sciences 32, 167–176.
Wang, Q., Ji, S., Salisbury, M.H., Xia, B., Pan, M., Xu, Z., 2005a. Pressure dependence and anisotropy of P-wave velocities in ultrahigh-pressure metamorphic rocks from the Dabie–Sulu orogenic belt (China). Implications for seismic properties of subducted slabs and origin of mantle reflections. Tectonophysics 398, 67–99.
Wang, Q., Ji, S., Salisbury, M.H., Xia, B., Pan, M., Xu, Z., 2005b. Shear wave properties and Poisson's ratios of ultrahigh-pressure metamorphic rocks from the Dabie–Sulu orogenic belt, China: implications for crustal composition. Journal of Geophysical Research 110, B08208. doi:10.1029/2004JB003435.
White, D.J., Milkereit, B., Salisbury, M.H., Percival, J.A., 1992. Crystalline lithology across the Kapuskasing uplift determined using in situ Poisson's ratio from seismic tomography. Journal of Geophysical Research 97 (B13) 19,993–20,006.
Williamson, P.R., 1991. A guide to the limits of resolution imposed by scattering in ray tomography. Geophysics 56, 202–207.
Zelt, B.C., Ellis, R.M., Zelt, C.A., Hyndman, R.D., Lowe, C., Spence, G.D., Fisher, M.A., 2001. Three-dimensional crustal velocity structure beneath the Strait of Georgia, British Columbia. Geophysical Journal International 44 (3), 695–712.
Zhu, X., Sixta, D.P., Angstman, B.G., 1992. Tomostatics: turning-ray tomography and static corrections. Geophysics: The Leading Edge 11, 12.